Young Neutron Stars and Their Environments
IAU Symposium, Vol. 218, 2004
F. Camilo and B. M. Gaensler, eds.

Shocks and Wind Bubbles Around Energetic Pulsars

Bryan M. Gaensler

Harvard-Smithsonian Center for Astrophysics, 60 Garden Street MS-6, Cambridge MA 02138, USA

Abstract. The Crab Nebula demonstrates that neutron stars can interact with their environments in spectacular fashion, their relativistic winds generating nebulae observable across the electromagnetic spectrum. At many previous conferences, astronomers have discussed, debated and puzzled over the complicated structures seen in the Crab, but have been limited to treating most other pulsar wind nebulae (PWNe) as simple calorimeters for a pulsar's spin-down energy. However, with the wealth of high-quality data which have now become available, this situation has changed dramatically. I here review some of the main observational themes which have emerged from these new measurements. Highlights include the ubiquity of pulsar termination shocks, the unambiguous presence of relativistic jets in PWNe, complicated time variability seen in PWN structures, and the use of bow shocks to probe the interaction of pulsar winds with the ambient medium.

1. Introduction

Pulsars are thought to be born with initial spin periods in the range 10–100 ms, implying initial rotational kinetic energies of the order of $\sim 10^{50}$ ergs. Timing observations readily establish that all isolated pulsars are spinning down; the implied *spin-down luminosity* is $\dot{E} = 4\pi^2 I \dot{P}/P^3$, where $I \equiv 10^{45}$ g cm^2 is the assumed moment of inertia for the neutron star, P is the star's rotational period and $\dot{P}$ is the spin period derivative. For typical young pulsars, we find spin-down luminosities in the range $\dot{E} \sim 10^{35} - 10^{39}$ ergs s^{-1}.

It is believed that most of this energy release ends up in a relativistic particle wind (see Melatos, these proceedings). At the interface where this wind interacts with its environment, a *pulsar wind nebula* (PWN) is formed. PWNe form an ideal laboratory for studying compact objects, relativistic shocks and particle acceleration, all key themes in a wide range of important astrophysical problems.

2. Overall Properties

While there are wide variations in PWN properties, three broad categories can be considered, loosely representing an evolutionary sequence (Fig. 1; van der Swaluw & Downes, these proceedings; van der Swaluw et al. 2004)

In the youngest systems ($t \lesssim 1000$ yr), $\dot{E}$ is approximately constant as a function of time; the PWN expands supersonically into unshocked low-density ejecta inside a surrounding expanding supernova remnant (SNR). In this phase

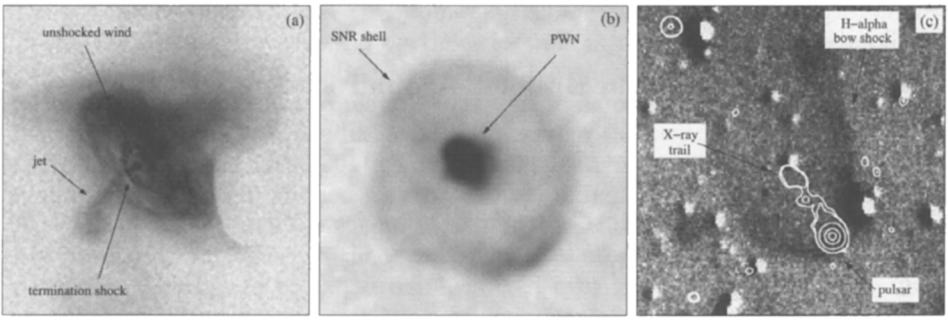

Figure 1. Examples of the three broad phases in PWN evolution. (a) *Chandra* X-ray image of the Crab Nebula; (b) ATCA radio image of SNR B0453–685 in the LMC; (c) AAO Hα (greyscale) and *Chandra* X-ray (contours) images of the bow shock powered by PSR B1957+20.

the radius of the PWN is small but is accelerating, with an approximate time-dependence $R \propto t^{6/5}$ (van der Swaluw et al. 2001, 2004). PWNe likely to be in this phase include the Crab Nebula (see Fig. 1[a]), and the PWN powered by PSR J1811–1925 in the young SNR G11.2–0.3 (Roberts et al. 2003).

In middle-aged systems ($t \sim$ 10–50 kyr), the interaction of the expanding supernova ejecta with their surroundings produces both forward and reverse shocks in the SNR. The latter collides with the pulsar wind shock, compressing and distorting the PWN. For a stationary pulsar in a spherically symmetric system, the PWN now expands subsonically. However, the effects of inhomogeneities in the surrounding interstellar medium (ISM), and of the pulsar's space velocity, can produce a significantly distorted PWN, with the pulsar near one end. Likely examples of PWNe in the process of interacting with their SNR's reverse shock include G327.7–1.1 (van der Swaluw & Downes, these proceedings) and B0453–685 in the Large Magellanic Cloud (Fig. 1[b]; Gaensler et al. 2003).

At later times ($t \gtrsim$ 100 kyr), the pulsar will move far from its birth site, and will eventually escape its SNR. The pulsar's motion is now supersonic, and its wind drives a bow shock, confined by ram pressure. Examples of bow shocks include those powered by PSRs B1957+20 ("the Black Widow") (Fig. 1[c]; Stappers et al. 2003) and J1747–2958 ("the Mouse") (Fig. 3[b]; Gaensler et al. 2004).

3. Crab-like Pulsar Wind Nebulae

In the earliest stages of evolution, a PWN is a quasi-spherical expanding wind bubble with a constant central energy source. Close to the pulsar, we expect that wind particles flow freely outward in all directions. This cold wind is not directly observable. At some distance (typically $\sim$ 0.1 pc) from the pulsar, this wind is confined by external pressure, and forms a *termination shock*. Particles are accelerated at this shock up to ultrarelativistic energies (see Arons, Lyubarsky, these proceedings). Downstream of the termination shock, the flow further decelerates and the gyrating particles emit synchrotron emission, forming the observable PWN.

For the Crab Nebula, the nebular magnetic field strength is high enough to cause significant synchrotron losses at high energies. We thus observe a

https://doi.org/10.1017/S0074180900180842 Published online by Cambridge University Press

centrally filled, linearly polarized source at all wavelengths, but whose extent in the optical and X-ray bands is progressively smaller than seen in the radio. It is sometimes claimed that at radio wavelengths (where the synchrotron lifetimes are longer than the age of the PWN), the PWN's luminosity traces the integrated history of the pulsar spin-down, while in X-rays (where the radiative lifetimes are short), the PWN luminosity traces the current energy output of the central star. However, while this is broadly true for the Crab Nebula, there are other young PWNe with much weaker magnetic fields, in which synchrotron losses are yet to dominate in X-rays (e.g., the PWN around PSR B1509–58; Gaensler et al. 2002a). Furthermore, interpretation of a PWN's radio emission as representing an integrated history of the system is complicated by adiabatic losses and the effects of the reverse shock interaction (Reynolds & Chevalier 1984).

In cases where synchrotron losses are significant in X-rays, one expects to see a spectral break somewhere between the radio and X-ray bands. Indeed in some cases this is observed; the break frequency can then be used to estimate the nebular magnetic field strength (e.g., Manchester et al. 1993). However, in other cases the field strength implied by such a break is unphysically large (e.g., Green & Scheuer 1992), while other PWNe appear to have multiple breaks in their spectra (e.g., Bock & Gaensler, these proceedings). Clearly spectral features in PWNe must be interpreted with caution, particularly when one considers that breaks in the spectrum can also be introduced by pulsar spin-down, or by intrinsic features in the injection spectrum (e.g., Woltjer et al. 1997).

3.1. Can We See Termination Shocks?

As mentioned above, we expect that there is an inner unshocked wind zone in young PWNe, bounded by a termination shock at which particles are accelerated. Indeed, the superb angular resolution of *Chandra* has revealed in several PWNe an underluminous region immediately surrounding the pulsar, surrounded by an X-ray bright termination shock, as shown in Figure 1(a). This clearly demarcates the point at which wind first interacts with its surroundings. In many cases this shock has a ring-like, rather than a spherical, geometry. This demonstrates that the synchrotron-emitting particles are concentrated into an equatorial flow around the pulsar spin-axis (see discussion by Melatos, these proceedings).

Once we have identified this axial symmetry, the position angle and eccentricity of this inner ring immediately provides the orientation of the pulsar in three dimensions, which can prove extremely useful in interpreting pulse profiles and in assessing the presence of "spin-kick" alignment (Ng & Romani 2004). Since the termination shock demarcates the point where the wind and nebular pressures balance, we can write:

$$\frac{\dot{E}}{\Omega r_w^2 c} = P_{nebula} \approx P_{fields} + P_{particles} \ , \qquad (1)$$

where Ω is the solid angle of the wind, r_w is the radius of the termination shock in the equatorial plane and P is the pressure. If we assume equipartition between fields and particles, Equation (1) then allows us to estimate the mean nebular field strength. Brightness variations are observed around the rims of these inner rings, as expected due to relativistic Doppler boosting. Fits to these

intensity variations allow us to directly determine the speed of the post-shock flow, $v = \beta c$; typical values are $0.4 \lesssim \beta \lesssim 0.6$ (e.g., Ng & Romani 2004)

3.2. Are Crab-like Pulsar Wind Nebulae Spherical?

Observations quickly demonstrate that young PWNe are not simple spherical bubbles (e.g., Fig. 1[a]). Many such sources show a clear axial symmetry, with significant elongation around the centrally-located pulsar. In cases where the termination shock can also be identified, this elongation is always perpendicular to the inner equatorial ring. It thus appears that the overall elongation of PWNe is an imprint of the pulsar spin-axis at much larger scales; if so, PWN morphologies then provide a simple way to infer the projected orientation of pulsar spin axes. The overall elongation of young PWNe may result from the winding up of nebular magnetic fields due to the pulsar's rotation, producing a toroidal field geometry which affects the dynamics of the PWN's expansion (Begelman & Li 1992; van der Swaluw 2003). However, in some cases there are striking collimated features extending up to ~ 5 pc from the pulsar (e.g., Gaensler et al. 2002a). Morphologically, these features appear to be high-velocity jets of particles, directed along the spin-axis. Indeed both proper motion and spectral measurements of these structures show them to have velocities $\beta \sim 0.3 - 0.6$ (Gaensler et al. 2002a; Hester et al. 2002). It is not yet clear what focuses these jets (see Melatos, these proceedings, for a detailed discussion); Komissarov & Lyubarsky (2003) have recently carried out simulations which show that hoop stress in the downstream flow above the spin axis may produce this collimation.

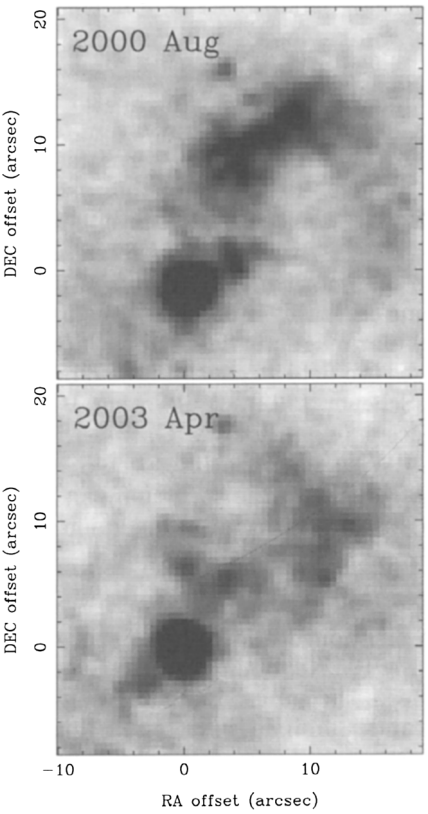

Figure 2. Multi-epoch *Chandra* images of the inner regions of the PWN powered by PSR B1509–58; the pulsar is the bright source at the origin (Gaensler et al., in preparation).

4. Time Variability

Multi-epoch data in the radio, optical, infrared, X-ray and possibly even gamma-ray bands all now demonstrate that PWNe show significant time variability (e.g., Hester et al. 2002; Pavlov et al. 2003; Ling & Wheaton 2003; Melatos, these proceedings). Much of the most rapid variability is observed near or even

https://doi.org/10.1017/S0074180900180842 Published online by Cambridge University Press

inside the termination shock (Fig. 2; Hester 1998), but complicated changes on timescales of months to years are seen in the outer parts of PWNe also (Pavlov et al. 2003; Mori et al., these proceedings). We are only just beginning to characterize these changes; clearly they represent a combination of phenomena, corresponding to particle acceleration, streaming instabilities, standing waves and turbulence. New theoretical attempts to model the time-dependence of pulsar winds and PWNe should provide important physical insight into the complicated processes being traced by these data-sets.

5. Bow-Shock Pulsar Wind Nebulae

Pulsar bow shocks provide a laboratory for studying pulsar winds under a particularly well-defined geometry. Furthermore, since pulsar positions, distances, spin-down luminosities and velocities are often well-constrained, these systems provide a physical situation which is highly amenable to detailed analysis. Until recently, few bow-shock systems were known. However, recent efforts have identified a series of new systems (e.g., Olbert et al. 2001; Gaensler et al. 2002b).

5.1. Theoretical Expectations

An idealized bow shock can be simply understood. The "stand-off distance" between the pulsar and the bow-shock apex is set by balance between ram pressure and wind pressure:

$$\frac{\dot{E}}{\Omega r_w^2 c} = P_{ram} = \rho V^2, \tag{2}$$

where ρ is the mass density of the ambient medium and V is the pulsar's space velocity. Furthermore, once one has measured r_w, the shape of the bow shock can be completely described by an analytic solution:

$$r(\theta) = r_w / \sin\theta \sqrt{3(1 - \theta/\tan\theta)}, \tag{3}$$

where $r(\theta)$ is the distance of the bow shock from the pulsar at an angle θ from the apex (Wilkin 1996). In practice, a bow-shock PWN has a double-shock structure, consisting of an outer forward shock and an inner termination shock, separated by a contact discontinuity (see Fig. 3[a]). Simulations suggest that the shape of the forward shock is still well-approximated by Equation (3).

5.2. Optical Emission from Bow Shocks

At the forward shock, we expect to see Hα emission, resulting from collisional excitation of neutrals in the ISM (e.g., Fig. 1[c]). Six bow shocks have been identified — five around radio pulsars and one around the isolated neutron star RX J1856.5–3754 (Chatterjee & Cordes 2002; Gaensler et al. 2002b). If V is known, the measured stand-off distance can be used to infer the ambient density via Equation (2). However, uncertainties in the inclination angle of the system ultimately limit the accuracy of such estimates (Gaensler et al. 2002b).

For the bow shocks around PSR J0437–4715 and RX J1856.5–3754, the morphology of the Hα emission is a good match to the analytic solution of

https://doi.org/10.1017/S0074180900180842 Published online by Cambridge University Press

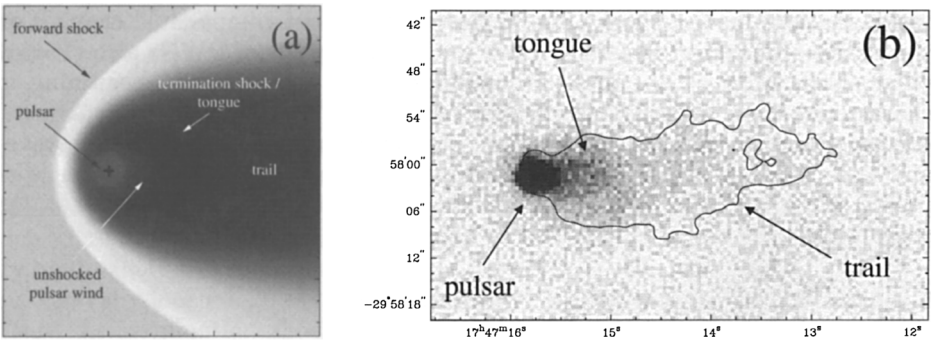

Figure 3. (a) Hydrodynamic simulation of a pulsar bow shock; the greyscale represents density on a logarithmic scale. (b) *Chandra* X-ray (greycale) and VLA radio (contour) data on the bow shock powered by PSR J1747–2958 ("the Mouse").

Equation (3) (e.g., van Kerkwijk & Kulkarni 2001). However, in the recently identified cases of PSRs B0740–28 and J2124–3358, there are significant deviations from this geometry, implying some combination of anisotropies in the pulsar wind flow (possibly corresponding to the torus/jet structures directly imaged in younger systems; see Fig. 1[a]) and structure in the ambient ISM (e.g., Gaensler et al. 2002b).

A typical pulsar space velocity of 500 km s^{-1} at a distance of 1 kpc corresponds to a proper motion of $\sim 0\farcs1$ yr^{-1}. The motion of the corresponding bow shock is easily detectable in just a few years. Indeed, Chatterjee & Cordes (2004) have recently measured motion of the "Guitar Nebula" powered by PSR B2224+65 over a seven-year baseline with *HST*, revealing significant changes in the structure and brightness of the optical emission from this PWN over this period. This and other multi-epoch studies of optical bow shocks will provide a unique measurement of fluctuations in the density of neutral gas in the ISM on scales $\sim 500 - 5000$ AU, filling a crucial gap between the turbulent power spectrum seen in H I on scales $\sim 0.1 - 200$ pc and the "tiny scale atomic structure" seen at scales $\sim 5 - 100$ AU.

5.3. Synchrotron Emission from Bow Shocks

Just as for Crab-like PWNe, for bow shocks we expect that the wind flows freely close to the pulsar, before decelerating at a termination shock, located inside the outer shock visible in Hα. Although the geometry may differ from the Crab-like case, it is reasonable to expect that the termination shock should also be a source of particle acceleration in bow shocks, and that we should thus see a central region in X-ray and radio synchrotron emission.

Indeed this has been confirmed in several sources, most notably around PSRs B1757–24 ("the Duck") (Kaspi et al. 2001), B1853+01 (Petre et al. 2002) and J1747–2958 (Fig. 3[b]; Gaensler et al. 2004). Until recently there were no cases in which both the forward and termination shocks had been identified in the same object. Since only the most energetic pulsars produce bright radio and X-ray PWNe (Gaensler et al. 2000; Gotthelf, these proceedings), and the radiation from such pulsars might also ionize their surroundings, this is not

https://doi.org/10.1017/S0074180900180842 Published online by Cambridge University Press

overly surprising (Chatterjee & Cordes 2002). However, in one case, that of the recycled binary pulsar B1957+20, an Hα bow shock and an enclosed X-ray PWN are both now clearly seen (Fig. 1[c]; Stappers et al. 2003). More instances of such systems need to be accumulated before we can hope to understand what controls the observability of each shock in such systems.

Observationally, the X-ray and radio emission from pulsar bow shocks forms an elongated trail behind the pulsar (Figs. 1[c] and 3[b]). Only for PSR B1957+20 have proper motion measurements confirmed that this trail aligns with the pulsar's direction of motion, but it is presumed that in other cases there is a similar alignment. Some authors have assumed these features to be synchrotron "wakes" left behind by the pulsar; in this case the length of the trail, combined with the pulsar's velocity, puts a lower limit on the system's age. However, in X-rays the radiative lifetimes are far too short to account for the observed extent of these trails; e.g. for PSR B1757–24, Kaspi et al. (2001) estimate a nebular magnetic field strength of $\sim 70\ \mu$G, which should result in a trail $\lesssim 1''$ in extent, in contrast to the $\sim 20''$ trail observed. One possibility is that there is a rapid flow behind the pulsar, which quickly transports particles downstream to form the trail (Wang et al. 1993; Kaspi et al. 2001).

A recent detailed comparison of *Chandra* and VLA data on the Mouse suggests an alternative interpretation. The Mouse shows *two* components to its bright synchrotron trail: a bright narrow "tongue" seen close to the pulsar, and a fainter trail, seen at larger distances downstream, as shown in Figure 3(b). Gaensler et al. (2004) combine the theory of ion-dominated pulsar winds with hydrodynamic simulations to show that the tongue likely represents the outer surface of the wind termination shock, analogous to the inner ring seen in *Chandra* images of the Crab Nebula, but stretched out due to ram pressure from the pulsar's motion. The fainter elongated trail then corresponds to synchrotron-emitting material seen further downstream.

It is important to note that the tongue feature seen for the Mouse resembles the *entire* trail seen for systems such as PSRs B1757–24 and B1957+20. I thus propose that the trails seen in these bow shocks represent the bright termination shock surrounding the pulsar, with the bulk of the PWN being much larger and much fainter, presumably due to a combination of adiabatic and synchrotron losses. If this interpretation is correct, then there is no need to invoke a rapid acceleration or collimation of the flow behind the pulsar; all positions in the tongue represent locations of fresh particle acceleration in the relativistic flow. Interestingly, *Chandra* images of bow shocks around PSR B1853+01 (Petre et al. 2002) and CXOU J061705.3+222127 (Olbert et al. 2001) both show suggestions of a bright tongue surrounded by a fainter trail, as seen for the Mouse. Deeper observations are needed to clarify these morphologies.

6. Conclusions

Some beautiful data-sets on PWNe are now letting us address a number of fundamental questions regarding these systems. We clearly now see the termination shock and post-shock flow for Crab-like PWNe, and the double-shock structure expected for bow-shock systems. We have learned how to use the morphology of these systems to infer a pulsar's spin axis, 3D orientation, and space veloc-

ity vector. We are beginning to explore the time-domain in PWN studies, with which we can probe the dynamics of a pulsar's interaction with its surroundings. While many questions remain to be answered, we observers no longer need to apologize for our data, and can happily provide our theorist colleagues with the measurements needed to properly address these issues. Clearly a new era in the study of pulsars and their winds is now well underway.

Acknowledgments. I thank all my PWN collaborators for their enthusiastic contributions to the work presented here. My research on PWNe is supported by NASA through SAO grants GO2-3079X, GO2-3074X, GO3-4068X, GO2-3075X and GO3-4063A, XMM-Newton Guest Observer grants NAG5-11376, NAG5-13087 and NAG5-13203, and LTSA grant NAG5-13032.

References

Begelman, M. C., & Li, Z.-Y. 1992, ApJ, 397, 187
Chatterjee, S., & Cordes, J. M. 2002, ApJ, 575, 407
— 2004, ApJ, 600, 51
Gaensler, B. M. et al. 2000, MNRAS, 318, 58
— 2002a, ApJ, 569, 878
— 2002b, ApJ, 580, L137
— 2003, ApJ, 594, L111
— 2004, ApJ, in press (astro-ph/0312362)
Green, D. A., & Scheuer, P. A. G. 1992, MNRAS, 258, 833
Hester, J. J. 1998, Mem. Soc. Ast. It., 69, 883
Hester, J. J. et al. 2002, ApJ, 577, L49
Kaspi et al. 2001, ApJ, 562, L163
Komissarov, S. S., & Lyubarsky, Y. E. 2003, MNRAS, 344, L93
Ling, J. C., & Wheaton, W. A. 2003, ApJ, 598, 334
Manchester, R. N., Staveley-Smith, L., & Kesteven, M. J. 1993, ApJ, 411, 756
Ng, C.-Y., & Romani, R. W. 2004, ApJ, 601, 479
Olbert, C. M. et al. 2001, ApJ, 554, L205
Pavlov, G. G. et al. 2003, ApJ, 591, 1157
Petre, R., Kuntz, K. D., & Shelton, R. L. 2002, ApJ, 579, 404
Reynolds, S. P., & Chevalier, R. A. 1984, ApJ, 278, 630
Roberts, M. S. E. et al. 2003, ApJ, 588, 992
Stappers, B. W. et al. 2003, Science, 299, 1372
van der Swaluw, E. 2003, A&A, 404, 939
van der Swaluw, E. et al. 2001, A&A, 380, 309
— 2004, A&A, submitted (astro-ph/0311388)
van Kerkwijk, M. H., & Kulkarni, S. R. 2001, A&A, 380, 221
Wang, Q. D., Li, Z.-Y., & Begelman, M. C. 1993, Nature, 364, 127
Wilkin, F. P. 1996, ApJ, 459, L31
Woltjer, L. et al. 1997, A&A, 325, 295